# Magnetic Mineralogy of Speleothems From Tropical-Subtropical Sites of South America

Plinio Jaqueto[1]*, Ricardo I. F. Trindade[1], Joshua M. Feinberg[2], Janine Carmo[1], Valdir F. Novello[3], Nicolás M. Stríkis[4], Francisco W. Cruz[3], Marília H. Shimizu[5] and Ivo Karmann[3]

[1] Departamento de Geofísica, Instituto de Astronomia, Geofísica e Ciências Atmosféricas, Universidade de São Paulo (USPmag), São Paulo, Brazil, [2] Department of Earth and Environmental Sciences, Institute for Rock Magnetism, University of Minnesota, Minneapolis, MN, United States, [3] Instituto de Geociências, Universidade de São Paulo, São Paulo, Brazil, [4] Departamento de Geoquímica, Universidade Federal Fluminense, Niterói, Brazil, [5] Center for Weather Forecasting and Climate Studies (CPTEC), National Institute for Space Research (INPE), Cachoeira Paulista, Brazil

Fe-bearing minerals are a tiny fraction of the composition of speleothems. They have their origin in the karst system or are transported from the drainage basin into the cave. Recent studies on the magnetism of speleothems focused on the variations of their magnetic mineralogy in specific time intervals and are usually limited to a single sample. In this study, we describe a database of environmental magnetism parameters built from 22 stalagmites from different caves located in Brazil (South America) at different latitudes, comprising different climates and biomes. The magnetic signal observed in these stalagmites is dominated by low-coercivity minerals ($\sim$20 mT) whose magnetic properties resemble those of the magnetite formed in pedogenic environments. Also, a comparison with few samples from soils and the carbonate from cave's walls shows a good agreement of the magnetic properties of speleothems with those of soil samples, reinforcing previous suggestions that in (sub-)tropical regimes, the dominant magnetic phase in speleothems is associated with the soil above the cave. Spearman's rank correlation points to a positive strong correlation between magnetic concentration parameters (mass-normalized magnetic susceptibility, natural remanent magnetization, anhysteretic remanent magnetization, and isothermal remanent magnetization). This implies that ultrafine ferrimagnetic minerals are the dominant phase in these (sub-)tropical karst systems, which extend across a diverse range of biomes. Although the samples are concentrated in the savannah biome (Cerrado) ($\sim$70%), comparison with other biomes shows a higher concentration of magnetic minerals in speleothem underlying savannahs and lower concentration in those underlying moist broadleaf forests (Atlantic and Amazon biome) and dry forests (Caatinga). Thus, rainfall, biome, and epikarst dynamics play an important role in the concentration of magnetic minerals in speleothems in (sub-)tropical sites and indicate they can be an important target for paleoenvironmental research in cave systems.

**Keywords: environmental magnetism, speleothem magnetism, South America, rock magnetism, karst system, stalagmites**
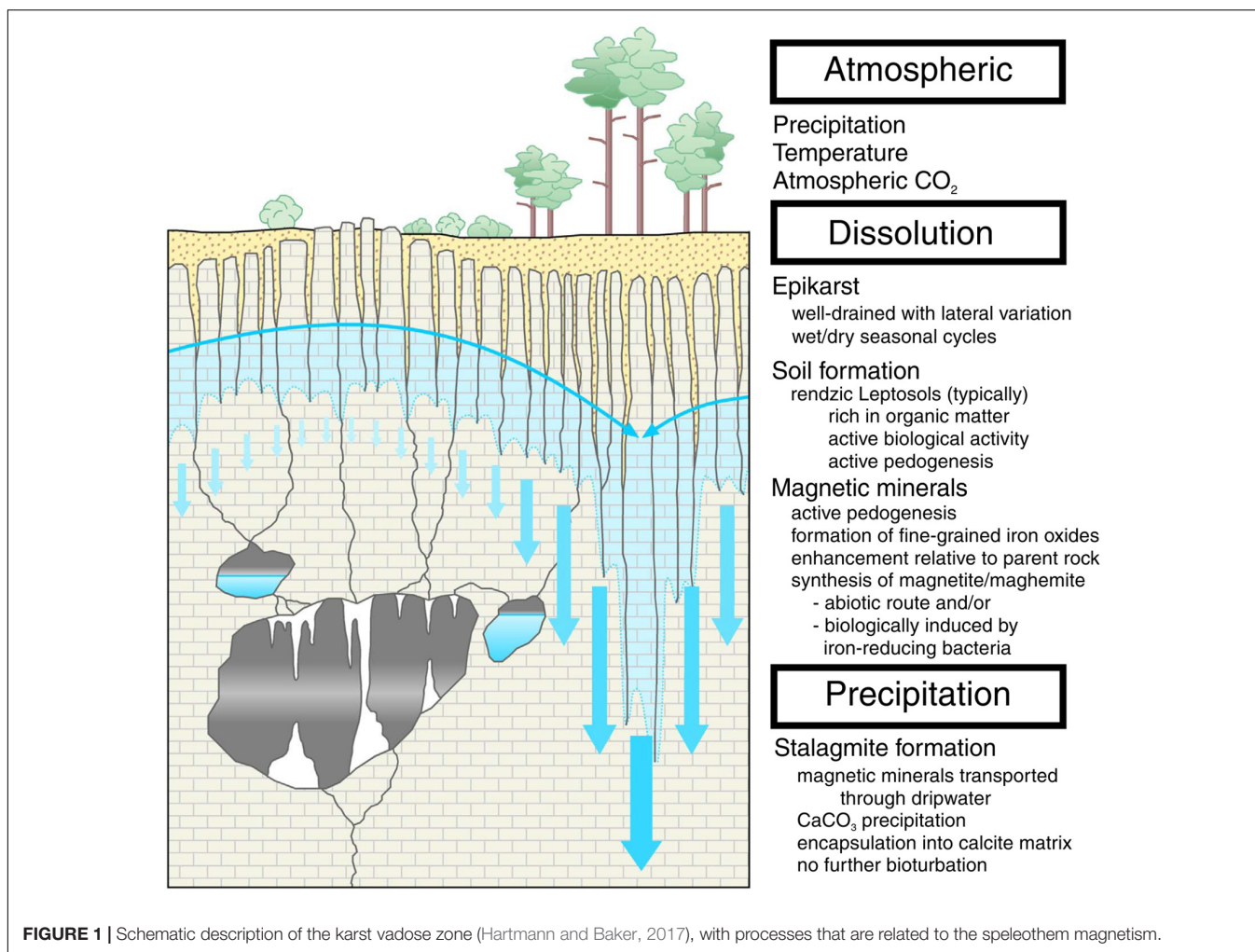
# INTRODUCTION

Speleothems, together with ice-cores, are among the best continental records used in paleoclimate and paleoenvironment reconstruction thanks to their precise chronology, widespread geographic distribution, and continuous growth. Environmental magnetic studies of speleothems show variations in the magnetic mineral concentrations that correlate with the decadal- to millennial-scale climate fluctuations at regional and/or global scales (**Table 1**; Xie et al., 2013; Bourne et al., 2015; Jaqueto et al., 2016; Zhu et al., 2017; Chen et al., 2019; Regattieri et al., 2019). The magnetic mineral assemblage and the relative concentration of different magnetic phases in speleothems can be interpreted in terms of **Figure 1**: (i) atmospheric processes (rainfall and temperature), (ii) epikarst processes (soil formation, vegetation change, soil $pCO_2$, and rate of carbonate dissolution), (iii) allochthonous detrital input, including flooding events or wind-blown particles, and (iv) modification of the magnetic mineralogy *in situ*, in the speleothem.

Precipitation is a major factor in speleothem formation. The karst system encompasses dissolution and precipitation regimes related to the carbonate–water interactions (Fairchild et al., 2006). The dissolution phase operates as a cascading system, comprising the atmosphere, the soil ecosystem, the epikarst, and the cave system itself (Fairchild and Baker, 2012). It involves the transformation of carbon dioxide gas $[CO_{2(g)}]$ that dissolves into water to form the species $[CO_{2(aq)}]$ reacting with water to form carbonic acid ($H_2CO_3$). This "weak" acid will progressively dissolve the limestone ($CaCO_3$), and this reaction will produce calcium ($Ca^{2+}$) and bicarbonate ($HCO_3^-$). At the precipitation phase, in the cave system, degassing of $CO_2$ will occur (when the solution is in contact with the cave atmosphere), and the secondary carbonate will form ($CaCO_3$), mainly calcite. The kinetics of the degassing reaction during calcite precipitation usually lasts from minutes to hours (Dreybrodt et al., 1997; Dreybrodt, 1999; Dreybrodt and Scholz, 2011) and favors the acquisition of detrital remanent magnetization. Furthermore, the absence of postdepositional perturbation, like bioturbation or

**TABLE 1 |** Speleothem magnetism studies and their respective resolution and interpretation.

| Study | Location | Climatology | Cave | Sample | Timespan | Average sample resolution | Magnetic parameter | Comparison | Interpretation |
|---|---|---|---|---|---|---|---|---|---|
| Xie et al., 2013 | China | Monsoonal, warm-wet summer and a cool-dry winter | Heshang Cave | HS4 | 0.15 ka–7.10 ka (6.94 ka) | 74 years | ARM/SIRM | Peatlands Hopanoids | Heavy rainfall resulted in the enhanced transport of coarse magnetic particles to the cave |
| Zhu et al., 2017 | China | Eastern Asian and Indian monsoon systems | Heshang Cave | HS4 | 0.15 ka–7.10 ka (6.94 ka) | 74 years | IRMsoft_flux | δ13C, Peatlands Hopanoids, ENSO variability, stalagmite BA03 – δ18O, and core V21-30 – δ18O foraminifera | Flux of soil-derived magnetic minerals correlate with rainfall amount and intensity |
| Bourne et al., 2015 | United States | Humid, temperate climate, and well-developed, midlatitude seasonality | Buckeye Creek Cave | BCC-010 | 58.71 ka–125.21 ka (66.49 ka) | 2015 years | IRMsoft, SIRM, IRMhard, S-ratio, IRM0.3T | δ13C, δ18O, Antarctic ice core $CO_2$, and Vostok ice core $CO_2$ | Changes in magnetite concentration as reflecting variations in local pedogenic processes, controlled by changes in regional precipitation |
| Jaqueto et al., 2016 | Brazil | South America Summer Monsoon with 90% of this amount falling | Pau D'Alho Cave | ALHO06 | 1891 CE–535 CE (1.35 ka) | 40 years | NRM, ARM, SIRM, HIRM, IRM_soft, S-ratio, ARM/SIRM | δ13C and δ18O | Concentration of magnetic minerals in the stalagmite is governed by soil erosion above the cave |
| Chen et al., 2019 | China | Subtropical monsoon climate, more than 65% rainfall falls during the monsoon season | Tangnei Cave | TN-1 | 77.9 ka to 82.3 ka (3.04 ka) | 15 years | Ms and Hc | δ13C, δ18O, and solar variability | Magnetic property in speleothems is interpreted to be related to regional precipitation |
| Regattieri et al., 2019 | Italy | Alpine climate, with precipitation correlated with southern Europe | Rio Martino Cave | RMD1 | 0.4 ka to 9.7 ka (9.3 ka) | 60 years | Magnetic susceptibility | δ13C, δ18O, growth rate, and lake level | Magnetic susceptibility concentration and carbon stable isotope ratio related to soil stability and pedogenesis |

**FIGURE 1 |** Schematic description of the karst vadose zone (Hartmann and Baker, 2017), with processes that are related to the speleothem magnetism.

compaction, helps conserve the magnetic remanence and allows the speleothem to retain reliable, directional, and paleointensity data (Lascu et al., 2016; Trindade et al., 2018; Zanella et al., 2018).

Soils play an important role in speleothem formation since the microbial activity of the soil and root respiration are the main factors controlling the $p$CO$_2$ in the solution, which in turn will drive carbonate dissolution (epikarst). In karst environments, soils are generally classified as Rendzina soils [Leptosols developed in carbonates (Jordanova, 2017)]. They develop over 10 to 100 years with a thin humic (A) horizon, overlying an incipient illuvial (B) horizon or the bedrock itself, and are often well drained with good aeration and a brown-to-black soil color (Jordanova, 2017). The combination of well-drained soil together with a large amount of organic and enhanced biological activity will promote an active pedogenesis producing fine-grained pedogenic iron oxides (SP/SSD magnetite fraction) with the magnetic enhancement of the soil relative to the host carbonate (**Figure 1**). So, the synthesis of pedogenic magnetite/maghemite via an abiotic route or via iron-reducing bacteria will be controlled by the characteristics of the biome and by the wetting and drying cycles in the soil (Jaqueto et al., 2016; Maxbauer et al., 2016a; Jordanova, 2017).

Transport of small-sized detrital particles derived from the soil into the cave system will occur through diffusive infiltration (**Figure 1**) along the fissures of the rock. These particles will be incorporated into the speleothem after reaching the top of the stalagmite by drip water (Bosch and White, 2004; Font et al., 2014; Bourne et al., 2015; Jaqueto et al., 2016; Zhu et al., 2017; Regattieri et al., 2019; Fu et al., 2021). Alternatively, detrital particles may reach the speleothems from sinking streams and from detrital material stored in the conduit system, or may result from flooded surface steams and episodic storm flows (Bosch and White, 2004; Feinberg et al., 2020). Also, detrital input close to cave entrances can be derived from wind-blown material (pollen and dust) (Fairchild et al., 2006). Finally, authigenic formation cannot be ruled out in some cases with the formation of goethite needles and biogenic magnetite at the precipitation site (Perkins, 1996; Strauss et al., 2013).

Most studies dealing with the environmental magnetism of speleothems interpret the variations in magnetic mineral concentration as a proxy for paleoprecipitation (**Table 1**). For example, Xie et al. (2013); Bourne et al. (2015), and Zhu et al. (2017) show a millennial-scale correlation between magnetic parameters and proxies for paleoprecipitation in

China and the southwest United States. Chen et al. (2019) used saturation magnetization (Ms) to track rainfall variation during MIS5a/4 transition, and the power spectrum of Ms showed that solar activity plays an important role in precipitation variation in southern China. More recently, Regattieri et al. (2019) linked climate proxies (with stable oxygen and carbon isotope) soil stability and evolution (magnetic parameters), and land-use on a Holocene speleothem from northern Italy.

In tropical sites, Jaqueto et al. (2016) suggested an inverse correlation at the multidecadal scale between paleoprecipitation and magnetic mineral concentration in a speleothem from western Brazil. In their model, the concentration of magnetic minerals in the stalagmite was governed by soil erosion and vegetation cover. A period of less rainfall (compared to the average) would be associated with less stable soils, resulting in higher fluxes of magnetic minerals into karst systems. Conversely, wetter periods would be associated with denser vegetation that inhibits the flux of the detritic material of the soil into the cave. In this case, the relation between paleoprecipitation and magnetic mineral concentration is not a direct one and depends on the soil dynamics and the vegetation cover in addition to the regional climate.

In the present study, we will explore the variations of magnetic mineralogy through different biomes in South America through a large speleothem magnetism database covering a wide range of latitudes (4°S to 24°S). Also, we present two detailed case studies where the magnetic signal of the speleothems is compared to the soil above the cave and the host carbonate to constrain the source of magnetic minerals inside the speleothems.

## REGIONAL SETTING

The central part of South America is dominated by warm and humid conditions, where the South America Summer Monsoon (SASM) is responsible for 70% of the rainfall from November to February (Garreaud et al., 2009; Campos et al., 2019). Present-day interannual climate variability is controlled by the El-Niño Southern Oscillation associated with the warmer conditions and rainfall below average on the northern part and wetter conditions on the southeastern part. Decadal and interdecadal variability is also present and is forced by the Pacific Decadal Oscillation with smaller amplitudes (Garreaud et al., 2009), while the paleoclimate reconstitution of the SASM based in $\delta^{18}O$ of the speleothems showed strong centennial variability linked to solar cycles (Novello et al., 2016).

The biomes at each karst system have different biodiversities like plant structure (trees vs. grasses), leaf type (broad vs. needles), plant spacing (forest vs. savannah), and climate that controls the organism type. Four main biomes are present in the main karst areas in Brazil (**Figure 2**; Ribeiro et al., 1983; Whitmore and Prance, 1987; Olson et al., 2001):
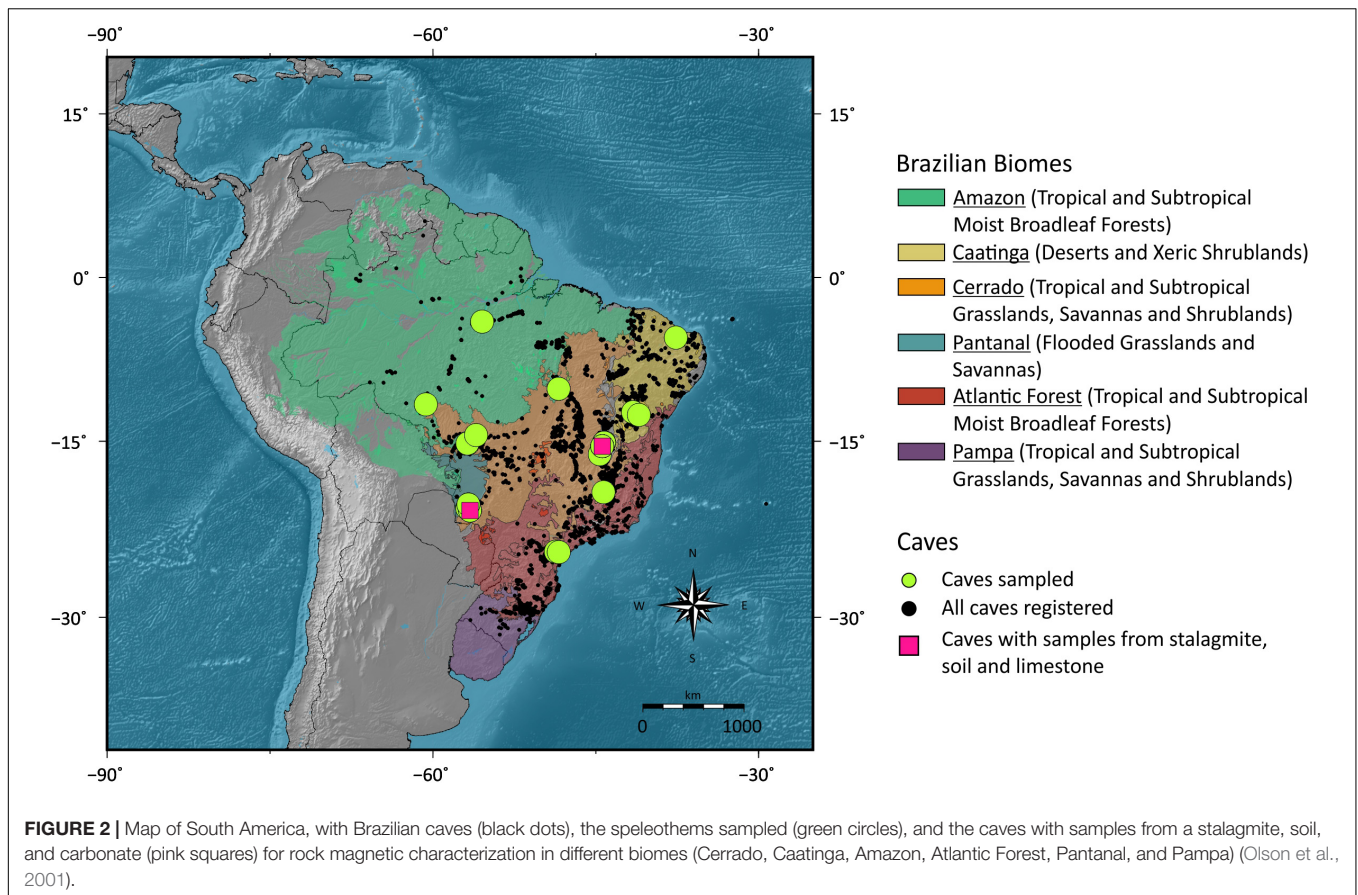
(1) Amazon biome (moist broadleaf forest), located in the north and northwestern part of Brazil, is characterized by low variability in temperature with a higher precipitation amount between 1,800 and 2,200 mm/year. Its ecoregion is classified as Neotropical, with high biodiversity; forest composition is dominated by evergreen trees with a dense high canopy; and the transition on its border is characterized by less dense understory.

(2) Cerrado biome (savannah), located in the Central part of Brazil, is characterized by seasonal rainfall, with a dry period during winter and a humid period in summer with average precipitation between 1,000 and 1,500 mm/year. Its ecoregion is classified as Neotropical, and it has a border with other biomes (Amazon, Atlantic, and Caatinga). The vegetation has characteristics of nutrient-poor, deep, and well-drained soils. Forest composition varies from an open field to a tall closed forest, which gives a distinctive biota feature in a mosaic fashion.

(3) Caatinga biome (dry forest), located in the northeastern part of Brazil, is characterized by a hot and dry climate with a precipitation amount between 700 and 750 mm/year (6–11 dry months). Its ecoregion is classified as Neotropical, and forest composition is considered heterogeneous, sparse, and diverse, ranging from low shrubby to tall caatinga forest.

(4) Atlantic biome (moist broadleaf forest), located in the southwestern part of Brazil along the southern coast, is characterized by high levels of rainfall between 1,600 and 1,800 mm/year. Its ecoregion is classified as Neotropical, with outstanding biodiversity in endemism. Forest ranges from coastal plains to the highest mountains, creating a vegetational gradient from shrubs to montane forests.

## MATERIALS AND METHODS

South American caves occur over a wide range of latitudes, and the speleothems within them act as climate archives extending back hundreds of millennia (Cruz et al., 2005). The choice of selected caves for this study was based on the availability of speleothems held at the Instituto de Geociências from Universidade de São Paulo and also the aim to sample different biomes (**Figure 2** and **Supplementary Figure 1**). In general, four specimens of each stalagmite were prepared with ∼7.5 mm of diameter and ∼10 mm of height (**Supplementary Figures 2–5**) (specimens do not have a radiometric age control). The resulting speleothem database (**Figure 2**) consists of 139 specimens (**Supplementary Table 1**), where 90 specimens were prepared from 22 different speleothems, 34 specimens from soil samples from the epikarst of 4 caves, and 15 specimens from the host carbonate of two different caves. In two specific sites (pink squares, **Figure 2**), Jaraguá Cave (21.09°S, 56.58°W) and Lapa dos Anjos (15.44°S, 44.40°W), the samples consist of the stalagmite, soil, and carbonate.

## ROCK MAGNETIC PARAMETERS

Rock magnetism techniques are commonly used in environmental studies aiming to understand three different

**FIGURE 2** | Map of South America, with Brazilian caves (black dots), the speleothems sampled (green circles), and the caves with samples from a stalagmite, soil, and carbonate (pink squares) for rock magnetic characterization in different biomes (Cerrado, Caatinga, Amazon, Atlantic Forest, Pantanal, and Pampa) (Olson et al., 2001).

parameters: composition, concentration, and granulometry (Evans and Heller, 2003). Magnetic concentration parameters include mass-normalized values of magnetic susceptibility ($\chi$), natural remanent magnetization (NRM), anhysteretic remanent magnetization (ARM), and isothermal remanent magnetization (IRM). Although they are referred to be concentration dependent, each of these parameters has different segments of grain size distribution and magnetic mineralogy in a sample. Magnetic susceptibility is the induced magnetization created by a small applied field, and in case of speleothems, it is influenced by ferromagnetic minerals, diamagnetic carbonates, and paramagnetic minerals from clays and silts. NRM is the total natural remanence held by low-coercivity minerals [10 s of mT by (titano)-magnetite/maghemite] as well as by high-coercivity minerals (100 s to 1,000 s of mT by hematite and goethite). Laboratory-induced remanences are useful for tracking a variety of other characteristics. ARM is the magnetization acquired during the application of a small DC field superimposed over an alternating field (AF) demagnetization step. ARM activates only those grains whose coercivities are less than the peak field reached during the AF step and that usually possess lower coercivity minerals such as magnetite and maghemite. IRM is the magnetization acquired after the application of a strong DC-pulsed field. Depending on the strength of the pulsed field, IRMs may include the saturation remanence of all low-coercivity minerals and portions of the hematite grain size distribution

(which typically requires field up to ~5 T to saturate). Goethite has a coercivity of >57 T (Rochette et al., 2005), and therefore, its remanence is not included in an IRM. Generally, IRM is interpreted as an indicator of magnetic mineral concentration. The ratio of ARM to IRM is often used as a granulometric tool, where higher ratios suggest a higher fraction of fine-grained, low-coercivity minerals capable of carrying a stable remanence (Maher, 2011). Another grain-size-dependent parameter is the median destructive field of ARM and IRM demagnetization curves, where higher values suggest smaller average grain sizes (Maher, 2011).

The S-ratio is a parameter used to quantify the fraction of an IRM that is held by low-coercivity minerals. Bloemendal et al. (1992) defined the S-ratio as:

$$Sratio = \frac{1}{2}\left(\frac{IRM_{@1T} - IRM_{@0.3T}}{IRM_{@1T}}\right)$$

where values close to 1 indicate that minerals with coercivities <300 mT dominate the remanence, while lower values suggest increasing contributions from higher coercivity minerals. Also, the remanence held by the high-coercivity fraction is termed as the "hard-isothermal remanent magnetization" (HIRM) and is calculated by multiplying the complement of the S-ratio by the $IRM_{1T}$ value (Maxbauer et al., 2016a).

## Methods

### Rock Magnetism Concentration Parameters

Rock magnetic measurements were performed on bulk specimens. Measurements of magnetic susceptibility ($\chi$), NRM, ARM, and IRM were conducted in a magnetically shielded room with an ambient noise field less than 500 nT at the Laboratório de Paleomagnetismo at the Universidade de São Paulo (USPMag).

The magnetic susceptibility of each specimen was measured 10 times at low frequency (F1: 976 Hz) in a Kappabridge MFK1 by AGICO Ltd., United Kingdom. Remanence measurements were carried out using a 2G Enterprises superconducting rock magnetometer (RAPID) (noise level $<5 \times 10^{-12}$ Am$^2$). The IRM consisted of applying two different fields using a pulse magnetizer by 2G enterprise (model 2660). The pulse-field was applied along the Z-axis for all specimens in fields of 1,000 mT and a back-field of $-300$ mT. At least two measurements were carried out in the RAPID magnetometer at each step.

### Unmixing of Magnetic Remanence

Analyses of the coercivity distribution are regularly applied in environmental magnetism studies to identify the different magnetic populations in natural sediments (Heslop, 2015; Roberts et al., 2019). The protocol for measuring ARM (incorporated into the RAPID system) was to apply a direct DC field of 0.03 mT superposed by an alternating field of 300 mT in the Z-axial coil at least two times, followed by a 300 mT demagnetization field in the quartz tube, and then an alternating field with 76 steps was performed, following a detailed stepwise demagnetization procedure (Egli, 2004a). The demagnetization of IRM was done in two of the four specimens for each stalagmite and followed the same steps as the ARM demagnetization (76 steps). Soil IRM intensities were close to the upper limit of the superconducting rock magnetometer ($>10^{-5}$ Am$^2$) causing higher standard deviations in the magnetization readings. For this reason, for these samples, we used the back-field IRM curves obtained in a vibrating sample magnetometer (VSM) by Princeton Measurements Corporation (model 3900) at the Institute for Rock Magnetism at the University of Minnesota. To comprehend the magnetic subpopulations and their differences in the varying latitudes and biomes, the skewed generalized Gaussian (SGG) functions were analyzed using the software MAX UnMix (Maxbauer et al., 2016b).

## RESULTS

## Rock Magnetism Concentration Parameters

Magnetic susceptibility was used to understand the contribution of different types of magnetic carriers in the karst system. The specimens were mass normalized, rather than volume normalized, to avoid issues arising from varying porosities. Speleothems and carbonates show similar low magnetic susceptibility values (**Figure 3**). These low values are due to the diamagnetic contribution from the calcite matrix and their low concentration of ferromagnetic material. The reference value of
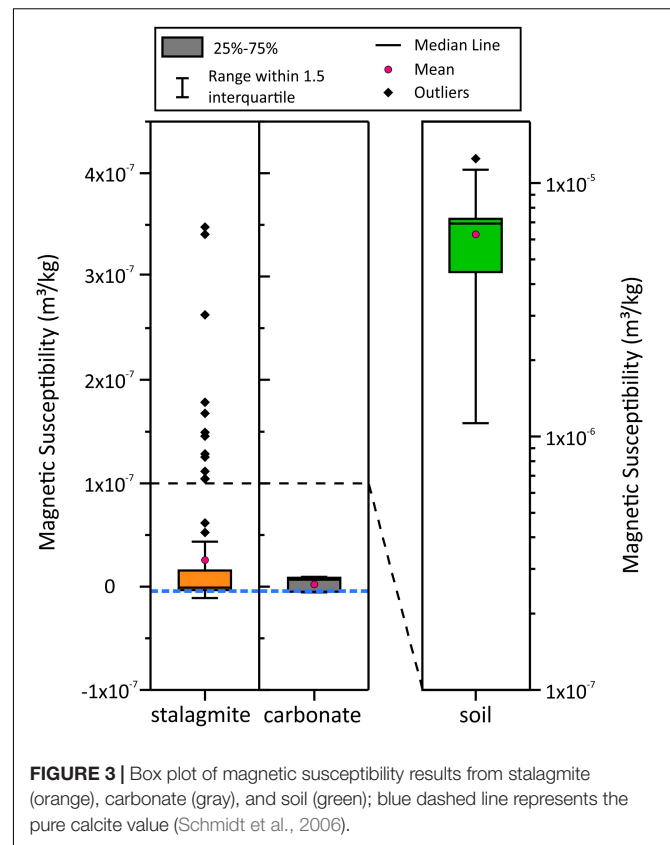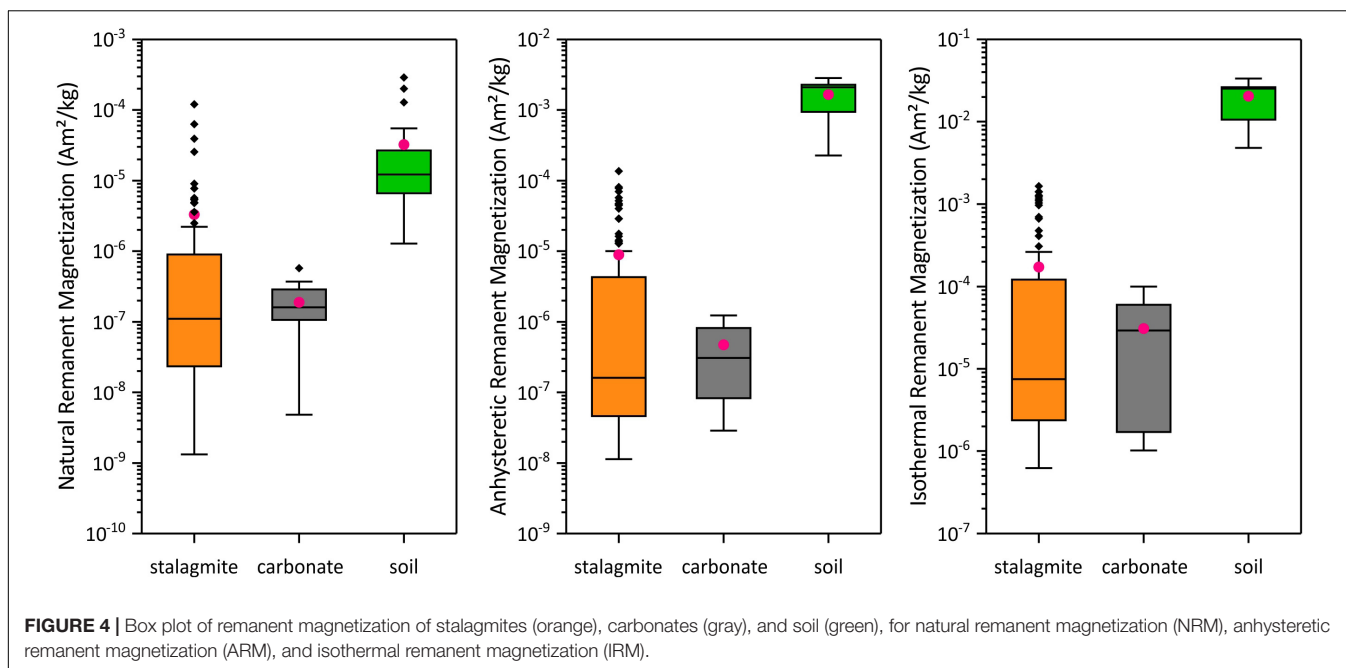


**FIGURE 3 |** Box plot of magnetic susceptibility results from stalagmite (orange), carbonate (gray), and soil (green); blue dashed line represents the pure calcite value (Schmidt et al., 2006).

susceptibility for pure calcite is $-4.46 \times 10^{-9}$ m$^3$/kg (Schmidt et al., 2006). The median value found for the stalagmites is $-2.00 \times 10^{-9} \pm 6.78 \times 10^{-8}$ m$^3$/kg, pointing to the calcite matrix. The median value for the carbonates is $6.71 \times 10^{-9} \pm 6.48 \times 10^{-9}$ m$^3$/kg. The soil has a magnetic susceptibility median value of $6.92 \times 10^{-6} \pm 3.12 \times 10^{-6}$ ml/kg, which is three to four orders of magnitude higher than that of calcite and carbonate (**Supplementary Table 1**).

The NRM, ARM, and IRM of all samples are shown in **Figure 4**. These results also indicate the contrast between the soil and the speleothems and the host carbonate, with lower median values for stalagmites NRM$_{stal}$: $1.10 \times 10^{-7} \pm 1.48 \times 10^{-5}$ Am$^2$/kg; ARM$_{stal}$: $1.61 \times 10^{-7} \pm 2.21 \times 10^{-5}$ Am$^2$/kg; IRM$_{stal}$: $7.48 \times 10^{-6} \pm 3.50 \times 10^{-4}$ Am$^2$/kg, a similar value for the carbonates NRM$_{carb}$: $1.60 \times 10^{-7} \pm 1.45 \times 10^{-7}$ Am$^2$/kg; ARM$_{carb}$: $3.07 \times 10^{-7} \pm 3.97 \times 10^{-7}$ Am$^2$/kg; IRM$_{carb}$: $2.93 \times 10^{-5} \pm 3.14 \times 10^{-5}$ Am$^2$/kg, and values of two to four orders of magnitude higher in the soil, with median values of NRM$_{soil}$: $1.22 \times 10^{-5} \pm 5.88 \times 10^{-5}$ Am$^2$/kg; ARM$_{soil}$: $2.11 \times 10^{-3} \pm 8.46 \times 10^{-4}$ Am$^2$/kg; IRM$_{soil}$: $2.52 \times 10^{-2} \pm 8.96 \times 10^{-3}$ Am$^2$/kg.

## S-Ratio and HIRM

The distributions of S-ratio (**Figure 5**) show a distinctive grouping behavior when compared to the concentration parameters. Soil and speleothems show a predominance

**FIGURE 4 |** Box plot of remanent magnetization of stalagmites (orange), carbonates (gray), and soil (green), for natural remanent magnetization (NRM), anhysteric remanent magnetization (ARM), and isothermal remanent magnetization (IRM).

of low-coercivity phases (stalagmite with median S-ratio: 0.97 ± 0.07; soil with median S-ratio: 0.99 ± 0.01) and a high-coercivity contribution being more prominent in the carbonate (median S-ratio: 0.70 ± 0.15). The HIRM, that is, the concentration of high-coercivity minerals, shows that these minerals are present with median values for stalagmites $7.0 \times 10^{-6} \pm 1.9 \times 10^{-5}$ Am$^2$/kg, carbonates $1.0 \times 10^{-5} \pm 1.1 \times 10^{-5}$ Am$^2$/kg, and soil $2.7 \times 10^{-4} \pm 1.6 \times 10^{-4}$ Am$^2$/kg (**Figure 5**). Although for soil the values are higher in content than carbonate and speleothems, they only represent ∼1% of the total IRM@1T, whereas, for carbonates and stalagmites, they represent 30% and 3%, respectively, of the total IRM@1T.

## Median Destructive Field of ARM and IRM

Demagnetization curves from stalagmites, carbonates, and soil indicate the presence of a low-coercivity magnetic phase in all specimens. Results from ARM have higher noise for stalagmites and carbonate due to the low-magnetization values close to the magnetometer noise level ($5 \times 10^{-12}$ Am$^2$), where only 63% of the stalagmite specimens could be analyzed. The IRM demagnetization curves also show the presence of a low-coercivity magnetic phase in all stalagmites and soil samples (**Supplementary Figure 6**). Conversely, the carbonates present higher coercivities.

Unmixing of the demagnetization curves of ARM and IRM was done using the MAX UnMix software (Maxbauer et al., 2016b), except when the noise dominates the signal. Only one component was fit for the whole dataset. Stalagmite and soil have similarly low values in coercivity (**Figure 6**) (stalagmite: MDF$_{ARM}$: 18.8 ± 1.1 mT; MDF$_{IRM}$: 20.3 ± 1.0 mT, soil: MDF$_{ARM}$: 17.7 ± 1.0 mT; MDF$_{IRM}$: 14.8 ± 1.0) and dispersion

(stalagmite, DP$_{ARM}$: 0.29 ± 0.02; DP$_{IRM}$: 0.39 ± 0.02; soil: DP$_{ARM}$: 0.28 ± 0.01; DP$_{IRM}$: 0.37 ± 0.01). The carbonate has median values of MDF$_{ARM}$: 37.6 ± 1.1 mT; MDF$_{IRM}$: 32.2 ± 1.1 mT; DP$_{ARM}$: 0.37 ± 0.04; DP$_{IRM}$: 0.49 ± 0.03. The results obtained of the median coercivity from both ARM and IRM measurements (**Figures 6, 7**) indicate that the magnetic signal of stalagmites is similar to that of the respective soil and contrasts with that of the host carbonate.

All speleothems irrespective of their location have coercivity values close to the detrital and pedogenic (plus extracellular) magnetite fields shown in **Figure 7**. The biplot of magnetic properties K$_{ARM}$/IRM by the median destructive field of ARM (MDF$_{ARM}$) also shows an agreement with fingerprint components: detrital pedogenic, detrital, detrital and extracellular magnetite, and pedogenic (DP, D, D+EX, and PD) (Egli, 2004b), supporting the soil-derived origin of the recorded magnetic signal. The results for carbonate data are not in agreement with the magnetic behavior of the speleothems and soil and are instead related to the magnetic mineral assemblage associated with their Neoproterozoic origin. Previous studies in stalagmites also found the same detrital/pedogenic magnetic component (Bourne et al., 2015; Jaqueto et al., 2016; Zhu et al., 2017), but they used median destructive field (ARM and IRM) and dispersion parameters instead of K$_{ARM}$/IRM. The K$_{ARM}$/IRM parameter was preferred instead of the dispersion parameter that does not have a clear physical meaning (Egli, 2004b).

## Two Case Studies: Jaraguá and Lapa Dos Anjos Caves

Two sites containing stalagmite, carbonate, and soil samples were chosen to refine this analysis. Lapa dos Anjos cave (15.44°S, 44.40°W) and Jaraguá cave (21.09°S, 56.58°W) are both
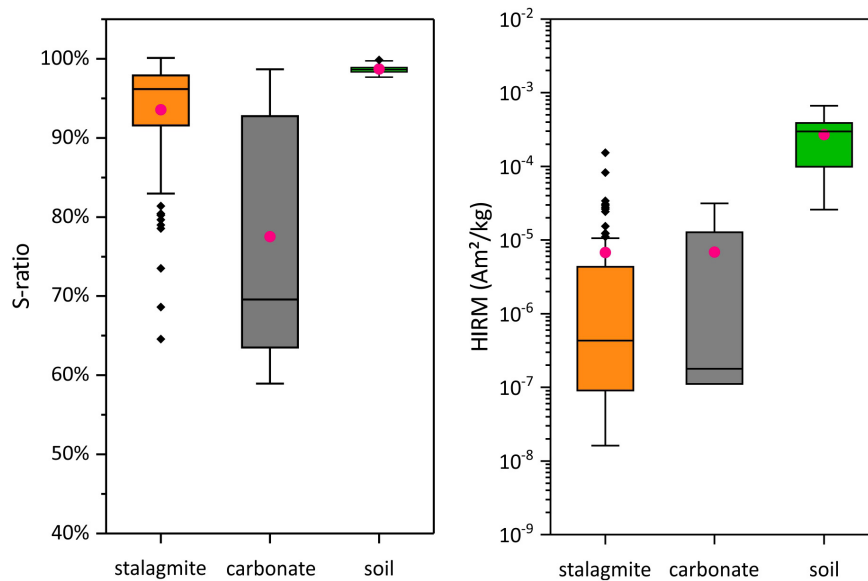
**FIGURE 5 |** Environmental magnetic parameters showing the fraction of remanence held by grains with coercivities <300 mT (S-ratio) and the remanence held by high-coercivity minerals (HIRM) for stalagmites (orange), carbonates (gray), and soil (green).
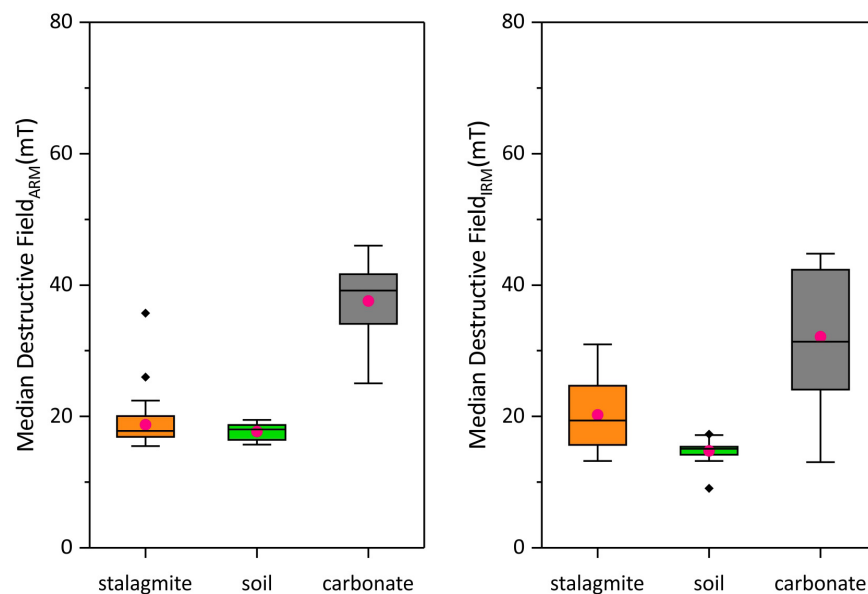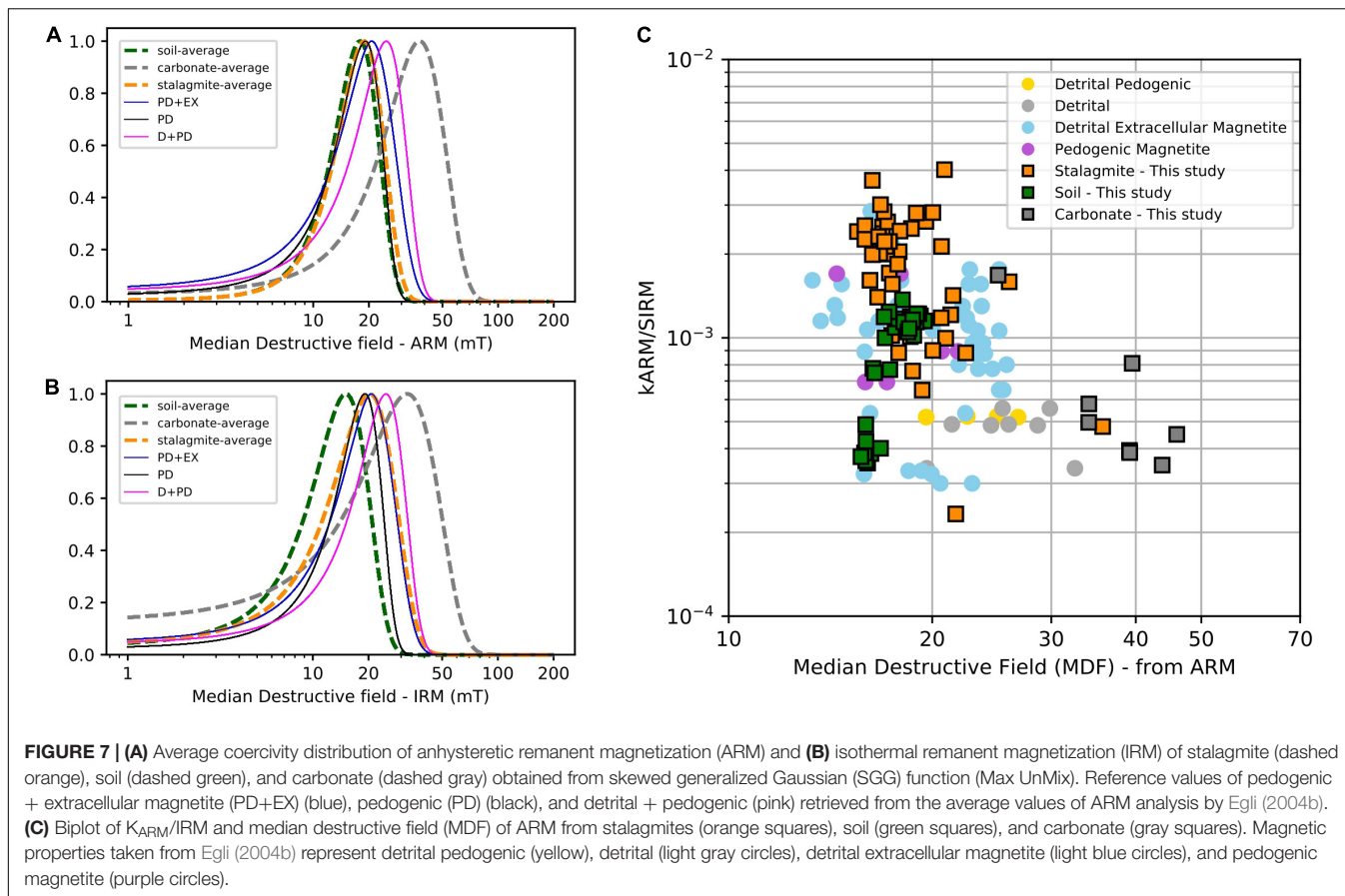


**FIGURE 6 |** Magnetic coercivity results from the adjustment of skewed generalized Gaussian (SGG) functions from the detailed demagnetization curves of ARM and IRM for stalagmites (orange), soil (green), and carbonates (gray).

located in the Cerrado biome. The average annual precipitation from 1979 to 2016 is 993.3 and 1402.7 mm/year, respectively (**Supplementary Figure 1**, Cerrado East#2 and Cerrado West #2). Both sites show a similar mean temperature of 23.0°C.

Stalagmites from both caves are considered "clean" (without "dirty" layers) (**Supplementary Figure 2**) and their median IRM values are $1.58 \times 10^{-6}$ Am$^2$/kg (Lapa dos Anjos) and $3.20 \times 10^{-6}$ Am$^2$/kg (Jaraguá cave) (**Figure 8**). Their host carbonates correspond to the Neoproterozoic formations of

Sete Lagoas (Lapa dos Anjos) and Bocaina (Jaraguá cave), and their median IRM values are $5.06 \times 10^{-5}$ Am$^2$/kg and $1.71 \times 10^{-6}$ Am$^2$/kg, respectively. The soil has median IRM values of $2.59 \times 10^{-2}$ Am$^2$/kg and $2.96 \times 10^{-2}$ Am$^2$/kg, respectively. Stalagmites and soil at both sites show high S-ratios consistent with magnetic mineral assemblages dominated by low-coercivity phases, with median values of 0.98 and 0.99 for Lapa dos Anjos cave and 0.97 and 0.99 for Jaraguá cave, respectively (**Figure 8**). By comparison, the carbonates at each site show

**FIGURE 7 | (A)** Average coercivity distribution of anhysteretic remanent magnetization (ARM) and **(B)** isothermal remanent magnetization (IRM) of stalagmite (dashed orange), soil (dashed green), and carbonate (dashed gray) obtained from skewed generalized Gaussian (SGG) function (Max UnMix). Reference values of pedogenic + extracellular magnetite (PD+EX) (blue), pedogenic (PD) (black), and detrital + pedogenic (pink) retrieved from the average values of ARM analysis by Egli (2004b). **(C)** Biplot of K$_{ARM}$/IRM and median destructive field (MDF) of ARM from stalagmites (orange squares), soil (green squares), and carbonate (gray squares). Magnetic properties taken from Egli (2004b) represent detrital pedogenic (yellow), detrital (light gray circles), detrital extracellular magnetite (light blue circles), and pedogenic magnetite (purple circles).

greater remanence contributions from high-coercivity minerals with S-ratios at Lapa dos Anjos of 0.64 and Jaraguá cave of 0.93.

The IRM demagnetization curves for stalagmites and soil yield lower median destructive fields, again showing the important role of lower coercivity minerals. The median MDF values for Lapa dos Anjos cave are 23.9 ± 3.1 mT and 15.1 ± 4.0 mT for stalagmites and soil, and for Jaraguá cave, the median MDF values are 19.7 ± 3.2 mT and 15.7 ± 1.3 mT. In contrast, the carbonate bedrocks for Lapa dos Anjos and Jaraguá caves have median MDF values of 43.4 ± 2.1 mT and 24.2 ± 5.9 mT, respectively (**Figure 8**). The coercivity values for stalagmite and soil from both caves have their magnetic properties in the same cluster as detrital, detrital pedogenic, and detrital extracellular magnetite (**Figure 7**). These results indicate that the dominant magnetic minerals in tropical stalagmites are mainly derived from overlying soils. Although magnetic minerals from host carbonate may be present, overall they have a low contribution to the magnetic signal.
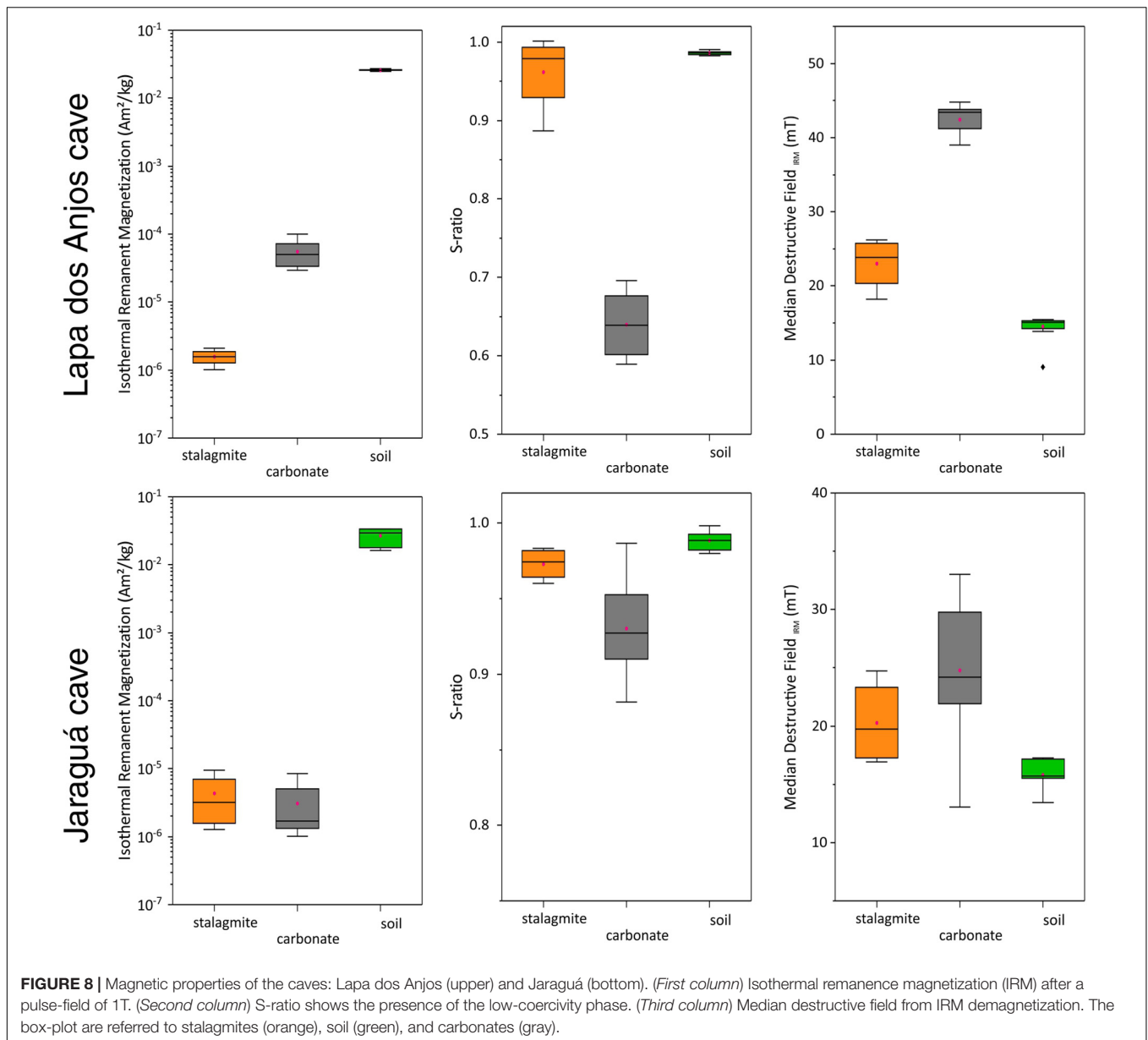
## MAGNETIC PARAMETERS AND BIOMES

### Spearman's Rank Correlation

To compare the results obtained within the database, we calculated the Spearman's rank correlation coefficients for 54 stalagmites specimens where IRM demagnetization was

performed. The following magnetic properties (see section "Rock Magnetic Parameters") were considered in the analysis: concentration parameters (magnetic susceptibility, NRM, ARM, and IRM), composition parameter (S-ratio), and granulometry parameters ($\chi_{ARM}$/SIRM and MDF$_{IRM}$) (**Figure 9**). Spearman's correlation is recommended to avoid a linear relationship since most magnetic parameters have non-Gaussian distributions (Hu et al., 2019).

In the speleothems, a strong correlation (>0.84) is found among the magnetic concentration parameters (susceptibility, NRM, ARM, and IRM) (**Figure 9**). This result supports the idea that the different magnetic concentration parameters in **Table 1** are essentially recording the same signal, with a predominance of ultrafine magnetite/maghemite in (sub-)tropical karst system. The strong correlation found using diverse rock magnetic parameters that respond differently to concentration, granulometry, types of magnetization, and magnetic mineralogy (see section "Rock Magnetic Parameters") shows that previous interpretations of the pedogenic origin of magnetic grains prevail tropical in karst systems and can be used to interpret local soil dynamics and rainfall regimes (Jaqueto et al., 2016; Fu et al., 2021).

The proportion of low-coercivity minerals indicated by S-ratio have a weak correlation coefficient (0.16–0.25) with magnetic concentration parameters. Antiferromagnetic minerals have been previously reported in stalagmites, mainly goethite and hematite
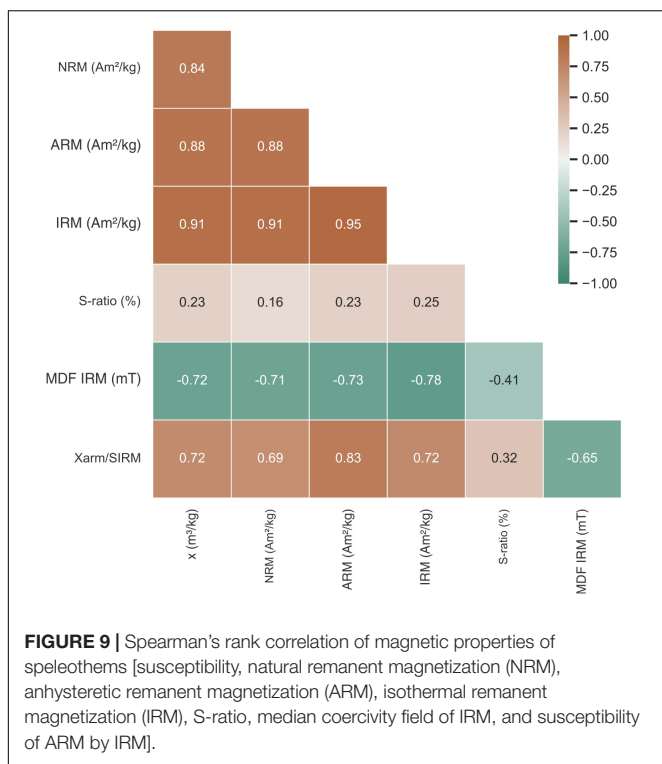
**FIGURE 8 |** Magnetic properties of the caves: Lapa dos Anjos (upper) and Jaraguá (bottom). (*First column*) Isothermal remanence magnetization (IRM) after a pulse-field of 1T. (*Second column*) S-ratio shows the presence of the low-coercivity phase. (*Third column*) Median destructive field from IRM demagnetization. The box-plot are referred to stalagmites (orange), soil (green), and carbonates (gray).

(Lascu and Feinberg, 2011; Strauss et al., 2013; Font et al., 2014); this positive weak correlation with S-ratio could indicate that the concentration parameters favor the input of low-coercivity minerals (magnetite and maghemite), and the changes observed in concentration parameters can be associated with a detrital concentration in drip water, instead of changes in mineralogy. So, changes in mineralogy tracked by S-ratio that correlate with magnetic concentration parameters would mean more complex dynamics in the karst system with changes of the dominant magnetic mineral phase, which is not found in (sub-)tropical regimes.

Coercivity parameters ($MDF_{IRM}$) have a strong negative correlation (0.71–0.78) with magnetic concentration parameters (**Figure 9**). This could indicate a better selection of magnetic mineral grain size and/or changes in soil oxidation reaction

(Ge et al., 2014). This is also evidenced by a negative moderate correlation (−0.41) with S-ratio, where a high coercivity could mean the presence of weathering (carbonate), detrital flood grains, and hematite (stable "old" soils). Granulometry parameter ($\chi_{ARM}$/SIRM) has a moderate negative correlation with $MDF_{IRM}$ (−0.65) and could be related to magnetic interaction between grains (Egli and Lowrie, 2002).

## The Influence of Biomes on Magnetic Mineral Formation

Biomes are defined by climate, leaf structure, leaf type, and plant spacing (Fairchild and Baker, 2012). In karst systems, the most common soils are Rendzina soils, with a characteristic of few centimeters and with relatively permeable bedrock, which
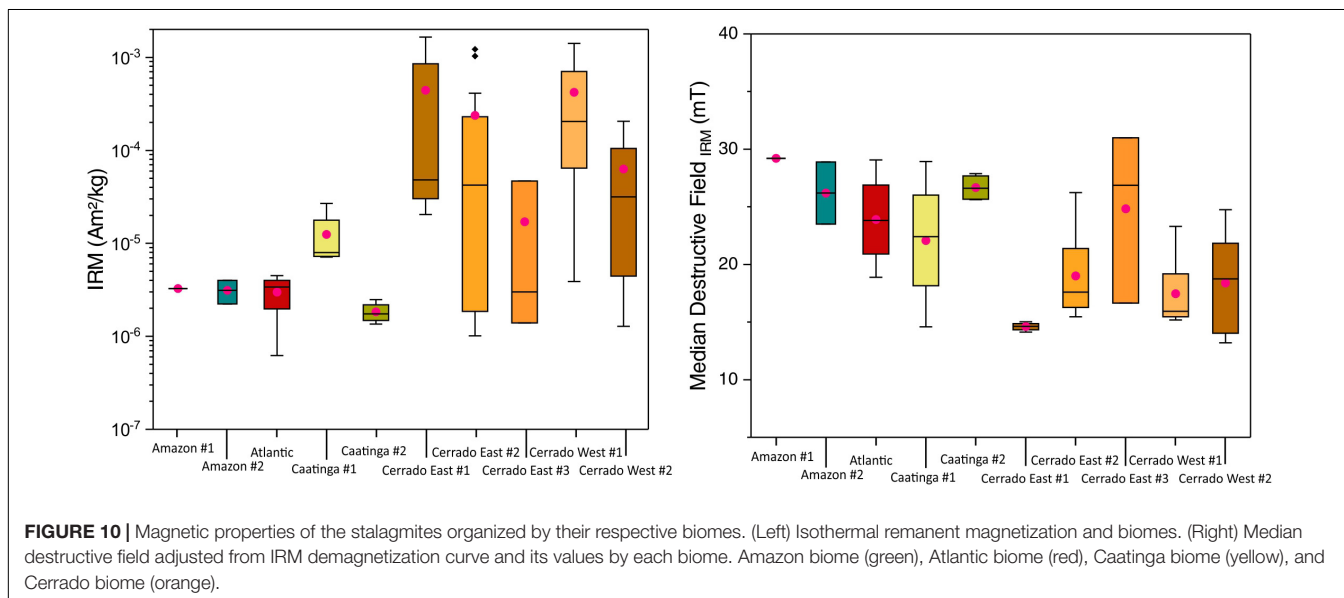
**FIGURE 9 |** Spearman's rank correlation of magnetic properties of speleothems [susceptibility, natural remanent magnetization (NRM), anhysteretic remanent magnetization (ARM), isothermal remanent magnetization (IRM), S-ratio, median coercivity field of IRM, and susceptibility of ARM by IRM].

allows the free drainage of soil profiles and anaerobic conditions. So, we grouped the samples by their biomes (**Figure 2** and **Supplementary Figure 1**) (Olson et al., 2001), compared with a magnetic concentration parameter (IRM) and coercivity to test for any correlation with different biomes (**Figure 10**). We chose these parameters based on the correlation between concentration parameters and coercivity due to their similarity with soil values.

The results from IRM grouped by biome (**Figure 10**) show a lower concentration in the Amazon, Atlantic, and Caatinga

biome, and higher concentrations and higher dispersions for the Cerrado biome. The coercivity values show a higher value for Amazon, Atlantic, and Caatinga biomes and lower values for Cerrado. Interestingly, these results are exactly consistent with the soil study of Maxbauer et al. (2017), which examined the magnetic properties of modern soils as a function of grassland (savannah) and forest biomes in mid-latitude Minnesota. The coherence observed between speleothem coercivity and IRM with the biomes may simply be a further expression of the close relationship between pedogenic processes at the surface and incorporation of pedogenic minerals into underlying karst features. Thus, in tropical settings such as Brazil, the magnetic mineral assemblages in speleothem may best be interpreted within the context of pedogenic processes.

- Cerrado biome (savannah shrubland): High concentration of magnetic minerals (median IRM of $1.40 \times 10^{-4}$ $Am^2$/kg) and low coercivity (median $MDF_{IRM}$ ∼18.4 mT) suggest a greater flux of magnetic minerals from the epikarst than other biomes.
- Caatinga (dry forest): Higher coercivity (median $MDF_{IRM}$ ∼24.4 mT) observed may be indicative of maghemitization (partial oxidation of magnetite) (Ozdemir and Dunlop, 2010) due to fewer dry/wet cycles, thereby inhibiting magnetic enhancement. Lower magnetic mineral concentrations are observed (median IRM of ∼$7.17 \times 10^{-6}$ $Am^2$/kg).
- Amazon and Atlantic biomes (moist broadleaf forest): Lower IRM values (median IRM of ∼$4.28 \times 10^{-6}$ $Am^2$/kg and ∼$5.05 \times 10^{-6}$ $Am^2$/kg, respectively) compared to Cerrado and higher coercivity values (median $MDF_{IRM}$ ∼27.7 mT and 23.9 mT, respectively) are observed. Two processes may explain this behavior: Enhanced maghemitization may increase the coercivity, while the prevalence of waterlogged soils and the concomitant dissolution of magnetic minerals could lower their



**FIGURE 10 |** Magnetic properties of the stalagmites organized by their respective biomes. (Left) Isothermal remanent magnetization and biomes. (Right) Median destructive field adjusted from IRM demagnetization curve and its values by each biome. Amazon biome (green), Atlantic biome (red), Caatinga biome (yellow), and Cerrado biome (orange).

concentration and diminish the transport of magnetic minerals to the cave system.

## SUMMARY AND CONCLUSION

This study presents a database of stalagmite magnetic properties, including parameters related to magnetic mineral composition and concentration and grain size. In two instances, we compared these values to those of the overlying soil and host carbonate. These results expand our knowledge of speleothem magnetic properties in tropical-subtropical regimes far beyond what could be achieved through the examination of one or more speleothems from a single cave. Additionally, this database provides robust evidence that the main magnetic component in Brazilian stalagmites is derived from soils overlying karst systems and that processes affecting pedogenic enhancement are reflected in these speleothems. The presence of low-coercivity magnetic minerals is pervasive across different latitudes and biomes. Median destruction field values from the demagnetization of IRMs show similarities between stalagmites and soil, whereas host carbonates showed consistently higher values. The fraction of remanence held by low-coercivity magnetic minerals as observed via the S-ratio (>90%) also shows this relationship.

Statistical analysis of stalagmite magnetic properties using Spearman's correlation shows a high correlation among rock magnetism concentration parameters (susceptibility, NRM, ARM, and IRM). Thus, although different parameters have been reported in the literature, they are essentially recording the same phenomena within (sub-) tropical zones. The weak correlation between magnetic concentration values with coercivity values shows that changes in mineralogy are not the main control in the karst system.

When compared within the four different biomes, the Cerrado biomes have a high concentration of magnetic minerals with coercivity values ~18.4 mT, whereas Caatinga, Amazon, and Atlantic biomes have a lower concentration of magnetic minerals and higher coercivity values of 24.4, 27.7, and 23.9 mT, respectively. This result is consistent with known trends in pedogenic processes and provides further evidence for the important role of pedogenic magnetite in Brazilian speleothems.

Future research on the fine-scale magnetic processes in karst systems would benefit from in-depth studies of soil profiles, constraining the physical and microbiological properties and periodically monitoring underlying caves, as is often done for oxygen and carbon isotope studies. This approach would allow researchers to explore how the flux of magnetic particles into cave environments varies with time and season across multiple biomes.

## DATA AVAILABILITY STATEMENT

The original contributions presented in the study are included in the article/**Supplementary Material**, further inquiries can be directed to the corresponding author/s.

## AUTHOR CONTRIBUTIONS

PJ, RT, JMF, VN, NS, FC, and IK conceived and planned the experiments. PJ performed the measurements. PJ, RT, JMF, JC, VN, and NS performed the analysis, drafted the manuscript, and designed the figures. MS and NS helped in climate series data and interpretation. FC and IK supervised the project. All authors contributed to the article and approved the submitted version.

## FUNDING

## ACKNOWLEDGMENTS

## SUPPLEMENTARY MATERIAL

The Supplementary Material for this article can be found online at: https://www.frontiersin.org/articles/10.3389/feart.2021.634482/full#supplementary-material

## REFERENCES

Bloemendal, J., King, J. W., Hall, F. R., and Doh, S. J. (1992). Rock magnetism of late Neogene and Pleistocene deep-sea sediments-relationship to sediment source, diagenetic processes, and sediment lithology. *J. Geophys. Res. Solid Earth* 97, 4361–4375. doi: 10.1029/91jb03068

Bosch, R. F., and White, W. B. (2004). *Lithofacies and Transport of Clastic Sediments in Karstic Aquifers*. Boston, MA: Springer, 1–22.

Bourne, M. D., Feinberg, J. M., Strauss, B. E., Hardt, B., Cheng, H., Rowe, H. D., et al. (2015). Long-term changes in precipitation recorded by magnetic minerals in speleothems. *Geology* 43, 595–598. doi: 10.1130/g36695.1

Campos, J., Cruz, F. W., Ambrizzi, T., Deininger, M., Vuille, M., Novello, V. F., et al. (2019). Coherent south american monsoon variability during the last millennium revealed through high-resolution proxy records. *Geophys. Res. Lett.* 46, 8261–8270. doi: 10.1029/2019gl082513

Chen, Q., Zhang, T. W., Wang, Y. T., Zhao, J. X., Feng, Y. X., Liao, W., et al. (2019). Magnetism signals in a stalagmite from Southern China and Reconstruction of paleorainfall during the interglacial-glacial transition. *Geophys. Res. Lett.* 46, 6918–6925. doi: 10.1029/2019gl082204

Cruz, F. W., Burns, S. J., Karmann, I., Sharp, W. D., Vuille, M., Cardoso, A. O., et al. (2005). Insolation-driven changes in atmospheric circulation over the past 116,000 years in subtropical Brazil. *Nature* 434, 63–66.

Dreybrodt, W. (1999). Chemical kinetics, speleothem growth and climate. *Boreas* 28, 347–356. doi: 10.1080/030094899422073

Dreybrodt, W., Eisenlohr, L., Madry, B., and Ringer, S. (1997). Precipitation kinetics of calcite in the system CaCO3-H2O-CO2: the conversion to CO2 by the slow process H++HCO3−>CO2+H2O as a rate limiting step. *Geochim. Cosmochim. Acta* 61, 3897–3904. doi: 10.1016/s0016-7037(97)00201-9

Dreybrodt, W., and Scholz, D. (2011). Climatic dependence of stable carbon and oxygen isotope signals recorded in speleothems: from soil water to speleothem calcite. *Geochim. Cosmochim. Acta* 75, 734–752. doi: 10.1016/j.gca.2010.11.002

Egli, R. (2004a). Characterization of individual rock magnetic components by analysis of remanence curves, 1. Unmixing natural sediments. *Studia Geophys. Geodaetica* 48, 391–446. doi: 10.1023/b:sgeg.0000020839.45304.6d

Egli, R. (2004b). Characterization of individual rock magnetic components by analysis of remanence curves. 2. Fundamental properties of coercivity distributions. *Phys. Chem. Earth* 29, 851–867. doi: 10.1016/s1474-7065(04)00129-9

Egli, R., and Lowrie, W. (2002). Anhysteretic remanent magnetization of fine magnetic particles. *J. Geophys. Res. Solid Earth* 107, 21.

Evans, M., and Heller, F. (2003). *Environmental Magnetism: Principles and Applications of Enviromagnetics.* Amsterdam: Elsevier.

Fairchild, I. J., and Baker, A. (2012). *Speleothem Science : From Process to Past Environments.* Hoboken, NJ: Wiley.

Fairchild, I. J., Smith, C. L., Baker, A., Fuller, L., Spotl, C., Mattey, D., et al. (2006). Modification and preservation of environmental signals in speleothems. *Earth Sci. Rev.* 75, 105–153. doi: 10.1016/j.earscirev.2005.08.003

Feinberg, J. M., Lascu, I., Lima, E. A., Weiss, B. P., Dorale, J. A., Alexander, E. C., et al. (2020). Magnetic detection of paleoflood layers in stalagmites and implications for historical land use changes. *Earth Planet. Sci. Lett.* 530:115946. doi: 10.1016/j.epsl.2019.115946

Font, E., Veiga-Pires, C., Pozo, M., Carvallo, C., Neto, A. C. D., Camps, P., et al. (2014). Magnetic fingerprint of southern Portuguese speleothems and implications for paleomagnetism and environmental magnetism. *J. Geophys. Res. Solid Earth* 119, 7993–8020. doi: 10.1002/2014jb011381

Fu, R. R., Hess, K., Jaqueto, P., Novello, V. F., Kukla, T., Trindade, R. I. F., et al. (2021). High-resolution environmental magnetism using the quantum diamond microscope (QDM): application to a tropical speleothem. *Front. Earth Sci.* 8:674.

Garreaud, R. D., Vuille, M., Compagnucci, R., and Marengo, J. (2009). Present-day South American climate. *Palaeogeogr. Palaeoclimatol. Palaeoecol.* 281, 180–195. doi: 10.1016/j.palaeo.2007.10.032

Ge, K. P., Williams, W., Liu, Q. S., and Yu, Y. (2014). Effects of the core-shell structure on the magnetic properties of partially oxidized magnetite grains: experimental and micromagnetic investigations. *Geochem. Geophys. Geosyst.* 15, 2021–2038. doi: 10.1002/2014gc005265

Hartmann, A., and Baker, A. (2017). Modelling karst vadose zone hydrology and its relevance for paleoclimate reconstruction. *Earth Sci. Rev.* 172, 178–192. doi: 10.1016/j.earscirev.2017.08.001

Heslop, D. (2015). Numerical strategies for magnetic mineral unmixing. *Earth Sci. Rev.* 150, 256–284. doi: 10.1016/j.earscirev.2015.07.007

Hu, P., Heslop, D., Viscarra Rossel, R. A., Roberts, A. P., and Zhao, X. (2019). Continental-scale magnetic properties of surficial Australian soils. *Earth Sci. Rev.* 203:103028. doi: 10.1016/j.earscirev.2019.103028

Jaqueto, P., Trindade, R. I. F., Hartmann, G. A., Novello, V. F., Cruz, F. W., Karmann, I., et al. (2016). Linking speleothem and soil magnetism in the Pau d'Alho cave (central South America). *J. Geophys. Res. Solid Earth* 121, 7024–7039. doi: 10.1002/2016jb013541

Jordanova, N. (2017). *Soil Magnetism: Applications in Pedology, Environmental Science and Agriculture.* Cambridge, MA: Academic Press, 1–445.

Lascu, I., and Feinberg, J. M. (2011). Speleothem magnetism. *Quat. Sci. Rev.* 30, 3306–3320. doi: 10.1016/j.quascirev.2011.08.004

Lascu, I., Feinberg, J. M., Dorale, J. A., Cheng, H., and Edwards, R. L. (2016). Age of the Laschamp excursion determined by U-Th dating of a speleothem geomagnetic record from North America. *Geology* 44, 139–142. doi: 10.1130/g37490.1

Maher, B. A. (2011). The magnetic properties of Quaternary aeolian dusts and sediments, and their palaeoclimatic significance. *Aeolian Res.* 3, 87–144. doi: 10.1016/j.aeolia.2011.01.005

Maxbauer, D. P., Feinberg, J. M., and Fox, D. L. (2016a). Magnetic mineral assemblages in gills and paleosols as the basis for paleoprecipitation proxies: a review of magnetic methods and challenges. *Earth Sci. Rev.* 155, 28–48. doi: 10.1016/j.earscirev.2016.01.014

Maxbauer, D. P., Feinberg, J. M., and Fox, D. L. (2016b). MAX UnMix: a web application for unmixing magnetic coercivity distributions. *Comput. Geosci.* 95, 140–145. doi: 10.1016/j.cageo.2016.07.009

Maxbauer, D. P., Feinberg, J. M., Fox, D. L., and Nater, E. A. (2017). Response of pedogenic magnetite to changing vegetation in soils developed under uniform climate, topography, and parent material. *Sci. Rep.* 7:10.

Novello, V. F., Vuille, M., Cruz, F. W., Strkís, N. M., de Paula, M. S., Edwards, R. L., et al. (2016). Centennial-scale solar forcing of the South American Monsoon System recorded in stalagmites. *Sci. Rep.* 6:24762. doi: 10.1038/srep24762

Olson, D. M., Dinerstein, E., Wikramanayake, E. D., Burgess, N. D., Powell, G. V. N., Underwood, E. C., et al. (2001). Terrestrial ecoregions of the worlds: a new map of life on Earth. *Bioscience* 51, 933–938. doi: 10.1641/0006-3568(2001)051[0933:teotwa]2.0.co;2

Ozdemir, O., and Dunlop, D. J. (2010). Hallmarks of maghemitization in low-temperature remanence cycling of partially oxidized magnetite nanoparticles. *J. Geophys. Res. Solid Earth* 115:B02101.

Perkins, A. M. (1996). Observations under electron microscopy of magnetic minerals extracted from speleothems. *Earth Planet. Sci. Lett.* 139, 281–289. doi: 10.1016/0012-821x(96)00013-1

Regattieri, E., Zanchetta, G., Isola, I., Zanella, E., Drysdale, R. N., Hellstrom, J. C., et al. (2019). Holocene Critical Zone dynamics in an Alpine catchment inferred from a speleothem multiproxy record: disentangling climate and human influences. *Sci. Rep.* 9:17829.

Ribeiro, J., Sano, S., Macedo, J., and da Silva, J. (1983). *Os Principais Tipos Fisionômicos da Região Dos Cerrados,* Vol. 21. Planaltina: Boletim de Pesquisa, EMBRAPA/CPAC.

Roberts, A. P., Hu, P. X., Harrison, R. J., Heslop, D., Muxworthy, A. R., Oda, H., et al. (2019). Domain state diagnosis in rock magnetism: evaluation of potential alternatives to the day diagram. *J. Geophys. Res. Solid Earth* 124, 5286–5314. doi: 10.1029/2018jb017049

Rochette, P., Mathe, P. E., Esteban, L., Rakoto, H., Bouchez, J. L., Liu, Q. S., et al. (2005). Non-saturation of the defect moment of goethite and fine-grained hematite up to 57 Teslas. *Geophys. Res. Lett.* 32: L22309.

Schmidt, V., Gunther, D., and Hirt, A. M. (2006). Magnetic anisotropy of calcite at room-temperature. *Tectonophysics* 418, 63–73. doi: 10.1016/j.tecto.2005.12.019

Strauss, B. E., Strehlau, J. H., Lascu, I., Dorale, J. A., Penn, R. L., and Feinberg, J. M. (2013). The origin of magnetic remanence in stalagmites: observations from electron microscopy and rock magnetism. *Geochem. Geophys. Geosyst.* 14, 5006–5025. doi: 10.1002/2013gc004950

Trindade, R. I. F., Jaqueto, P., Terra-Nova, F., Brandt, D., Hartmann, G. A., Feinberg, J. M., et al. (2018). Speleothem record of geomagnetic South Atlantic Anomaly recurrence. *Proc. Natl. Acad. Sci. U.S.A.* 115, 13198–13203. doi: 10.1073/pnas.1809197115

Whitmore, T. C., and Prance, G. T. (1987). *Biogeography and Quaternary History in Tropical America.* Oxford: Clarendon Press.

Xie, S. C., Evershed, R. P., Huang, X. Y., Zhu, Z. M., Pancost, R. D., Meyers, P. A., et al. (2013). Concordant monsoon-driven postglacial hydrological changes in

peat and stalagmite records and their impacts on prehistoric cultures in central China. *Geology* 41, 827–830. doi: 10.1130/g34318.1

Zanella, E., Tema, E., Lanci, L., Regattieri, E., Isola, I., Hellstrom, J. C., et al. (2018). A 10,000 yr record of high-resolution paleosecular variation from a flowstone of Rio Martino Cave, Northwestern Alps, Italy. *Earth Planet. Sci. Lett.* 485, 32–42. doi: 10.1016/j.epsl.2017.12.047

Zhu, Z. M., Feinberg, J. M., Xie, S. C., Bourne, M. D., Huang, C. J., Hu, C. Y., et al. (2017). Holocene ENSO-related cyclic storms recorded by magnetic minerals in speleothems of central China. *Proc. Natl. Acad. Sci. U.S.A.* 114, 852–857. doi: 10.1073/pnas.1610930114